How to cite: *Angew. Chem. Int. Ed.* **2024**, *63*, e202312123
doi.org/10.1002/anie.202312123

Time-Resolved Spectroscopy

Ultrafast Surface-Specific Spectroscopy of Water at a Photoexcited TiO_2 Model Water-Splitting Photocatalyst

Ellen H. G. Backus, Saman Hosseinpour, Charusheela Ramanan, Shumei Sun, Simon J. Schlegel, Moritz Zelenka, Xiaoyu Jia, Maximilian Gebhard, Anjana Devi, Hai I. Wang, and Mischa Bonn*

Abstract: A critical step in photocatalytic water dissociation is the hole-mediated oxidation reaction. Molecular-level insights into the mechanism of this complex reaction under realistic conditions with high temporal resolution are highly desirable. Here, we use femtosecond time-resolved, surface-specific vibrational sum frequency generation spectroscopy to study the photo-induced reaction directly at the interface of the photocatalyst TiO_2 in contact with liquid water at room temperature. Thanks to the inherent surface specificity of the spectroscopic method, we can follow the reaction of solely the interfacial water molecules directly at the interface at timescales on which the reaction takes place. Following the generation of holes at the surface immediately after photoexcitation of the catalyst with UV light, water dissociation occurs on a sub-20 ps timescale. The reaction mechanism is similar at pH 3 and 11. In both cases, we observe the conversion of H_2O into Ti–OH groups and the deprotonation of pre-existing Ti–OH groups. This study provides unique experimental insights into the early steps of the photo-induced dissociation processes at the photocatalyst-water interface, relevant to the design of improved photocatalysts.

Introduction

Finding clean and renewable energy sources to replace fossil fuels has attracted much attention in the past few decades, as a requirement for the sustainable development of society. Direct hydrogen generation on TiO_2 by photocatalytic water dissociation using sunlight was first proposed around 50 years ago.[1] In recent years, intensive studies have been devoted, amongst others, to modifying the photocatalysts to utilize a broader range of the solar spectrum and to make the water-splitting process more efficient (see, for example, the recent reviews[2–4]). Although TiO_2 is not a very efficient catalyst, it is widely used as a model system to understand the fundamentals of light-induced surface reactions, owing to its stability and relative simplicity. Atomic-scale insights into the modes of interaction between water and TiO_2 under well-defined conditions have contributed substantially to our understanding of this complex system (see, e.g.[5–7]). Understanding the reaction mechanism of photocatalytic water splitting has been a research focus both experimentally and theoretically. In general, for hydrogen generation on a semiconductor, the hole-mediated oxidation reaction is often the rate-determining step:[8] $Ti–OH_2 + h^+ \rightarrow Ti–OH + H^+$.[9,10] Subsequently, by adsorbing another hole, Ti–OH could turn into Ti–O. In two additional reaction steps, involving another water molecule and two holes, oxygen could be produced.[9,10] Valdes et al. used density functional theory (DFT) to conclude that, for rutile TiO_2, the initial formation of the adsorbed hydroxyl group is the rate-limiting step in oxygen production.[9] A DFT-based first-

[*] E. H. G. Backus, M. Zelenka
University of Vienna, Faculty of Chemistry, Institute of Physical Chemistry
Währinger Straße 42, 1090 Vienna (Austria)
E-mail: ellen.backus@univie.ac.at

E. H. G. Backus, S. Hosseinpour, C. Ramanan, S. Sun, S. J. Schlegel, X. Jia, H. I. Wang, M. Bonn
Max Planck Institute for Polymer Research
Ackermannweg 10, 55128 Mainz (Germany)

C. Ramanan
Department of Physics and Astronomy, Faculty of Sciences, Vrije Universiteit Amsterdam
De Boelelaan 1081, 1081 HV Amsterdam (The Netherlands)

M. Gebhard, A. Devi
Inorganic Materials Chemistry, Ruhr-University Bochum
Universitätsstraße 150, 44801 Bochum (Germany)

H. I. Wang
Nanophotonics, Debye Institute for Nanomaterials Science, Utrecht University
Princetonplein 1, 3584 CC Utrecht (The Netherlands)

S. Hosseinpour
Current address: Institute of Particle Technology (LFG), Friedrich-Alexander-Universität-Erlangen-Nürnberg (FAU)
Cauerstraße 4, 91058 Erlangen (Germany)

principles molecular dynamics simulation by Chen et al. showed that for anatase TiO_2 at pH below the point of zero charge, the proton transfer step in the first reaction is limiting, i.e. $Ti–OH_2 \rightarrow Ti–OH^- + H^+$. Above the point of zero charge, electron transfer ($Ti–OH^- + h^+ \rightarrow Ti–OH$) is rate limiting as the TiO_2 surface is covered with hydroxyl anions in this case.[10] The proton transfer barrier is higher than that for the electron transfer.[10] A more recent molecular dynamics simulation by Wang et al. has indicated that for the water/TiO_2(110) interface, all steps in the oxygen evolution reaction are slow due to the low concentration of surface-reaching photo-generated holes.[11] Lately, Ma et al. reported in a combined experimental and theoretical study for anatase TiO_2(001) that an internal hydrogen bond network facilitates water splitting by lowering the dissociation energy barrier and by promoting the coupled proton and hole transfer.[12] They mentioned that their study at low temperature and low pressure provides meaningful insights for water splitting at room temperature in liquid aqueous environments.

Yet, experimental studies on the water dissociation dynamics under realistic conditions with a macroscopic (i.e. bulk) amount of water in contact with TiO_2 are very scarce. This is in part due to the challenge of experimentally addressing the reactions specifically at the interface between bulk water and the TiO_2 surface. In most measurement techniques, the signal from the interfacial molecules in the first few layers next to the interface is overwhelmed by the signal generated in the bulk water (all water further away than a few molecular layers from the interface) or bulk TiO_2. Sum frequency generation spectroscopy (SFG) offers inherent surface-specificity, and can thus be an ideal tool to probe the water molecules at the interface between bulk water and bulk TiO_2, as has been demonstrated for water in contact with a few nm thin TiO_2 film,[13] anatase TiO_2,[14] and water in contact with amorphous TiO_2.[15] In the latter two studies, distinct spectroscopic features could be linked to specific sub-ensembles of O–H groups, i.e., different types of water molecules and Ti–OH groups, present in the interfacial region, paving the way to study photo-induced reaction dynamics. An alternative method, as reported in literature, to study interfacial layers in the presence of a bulk amount of water, is surface X-ray diffraction (SXRD). For anatase (101), it has been concluded from SXRD experiments that a mixture of molecular H_2O (25 %) and OH groups (75 %) are present at the interface.[16] However, these previous SXRD and SFG studies on the TiO_2-water interface only focused on the static structure. No information about the relevant reaction mechanism and corresponding timescales of the water dissociation processes could be obtained.

To obtain experimental insights into the reaction mechanism and the timescale of reaction steps of photocatalytic water dissociation, we report here the first time-resolved SFG experiments on the water-TiO_2 interface. In these experiments, a thin film of amorphous TiO_2 deposited on CaF_2 is excited with a 310 nm UV laser pulse of a few 100 fs in duration. The structural changes at the interface are followed by SFG spectroscopy using the O–H stretch vibration as markers of the water molecules and interfacial Ti–OH groups. Changing the time delay between the UV pulse and SFG probe pair allows us to follow the sub-picosecond dynamics at the TiO_2/water interface. As the hole-mediated oxidation reaction is the rate-determining reaction step, we first use transient absorption spectroscopy to select samples with trapped surface-holes. Complementary terahertz spectroscopy experiments provide information about the mobility of the light-induced charge carriers. Our results reveal the hole-mediated water dissociation at the interface of amorphous TiO_2 and bulk water on a sub-20 ps timescale.

Results and Discussion

Figure 1a shows UV/Vis absorption spectra of three different atomic-layer-deposited (ALD) thin TiO_2 films on CaF_2 (2 mm). See Supporting Information for details about the sample preparation. The CaF_2 substrate has negligible absorption between 250 and 900 nm. All three TiO_2 samples show a strong absorbance below 400 nm caused by TiO_2, but samples 2 and 3 show an additional apparent absorption at 475 nm. The observed differences above 400 nm are an optical artifact caused by interference of multiple reflections at the air-TiO_2 and TiO_2-CaF_2 interfaces resulting in apparent minima (e.g. 400 and 650 nm) and maxima (e.g. 475 nm) not caused by absorption features in the TiO_2 at these specific wavelengths.[17,18] The different layer thickness of roughly 75 nm (sample 1) vs 150 nm (sample 2/3) explains the different interference patterns in the optical spectra and the difference in absorbance intensity below 400 nm. These interference effects might hide minor differences in the spectrum due to, for example, different doping levels. Besides UV/Vis, the samples are characterized with Raman spectroscopy (see SI) to determine their structure. As depicted in the inset in Figure 1a, sample 2 and 3 show clear peaks at 143, 401, 521, and 633 cm^{-1} originating from crystalline anatase TiO_2.[19] These peaks are present on a broad band assigned to amorphous TiO_2. As the Raman spectrum of sample 1 shows only this broad band, we conclude that sample 1 is amorphous, while samples 2 and 3 have also a significant fraction of crystallinity. The small signal at 319 cm^{-1} present in all Raman spectra can be assigned to the CaF_2 substrate. The difference in crystallinity is most likely due to the impact of the plasma pulse and temperature variations in the sample during the ALD.[20] Thicker films are taking longer time, probably heating up more. XPS analysis of the samples shows no significant difference in composition between samples 1 and 2, comprising Titanium and Oxygen. Sample 3 has trace amounts of Al and Si present, probably due to contamination during the layer preparation due to residual precursor fragments from earlier depositions.

As reported in literature,[21,22] transient absorption (TA) spectroscopy[23] in the visible/near-infrared region is very sensitive to the type of carriers present in a semiconductor. As such, we performed 315 nm excitation and monitored the transient changes between 500 and 900 nm. Experimental

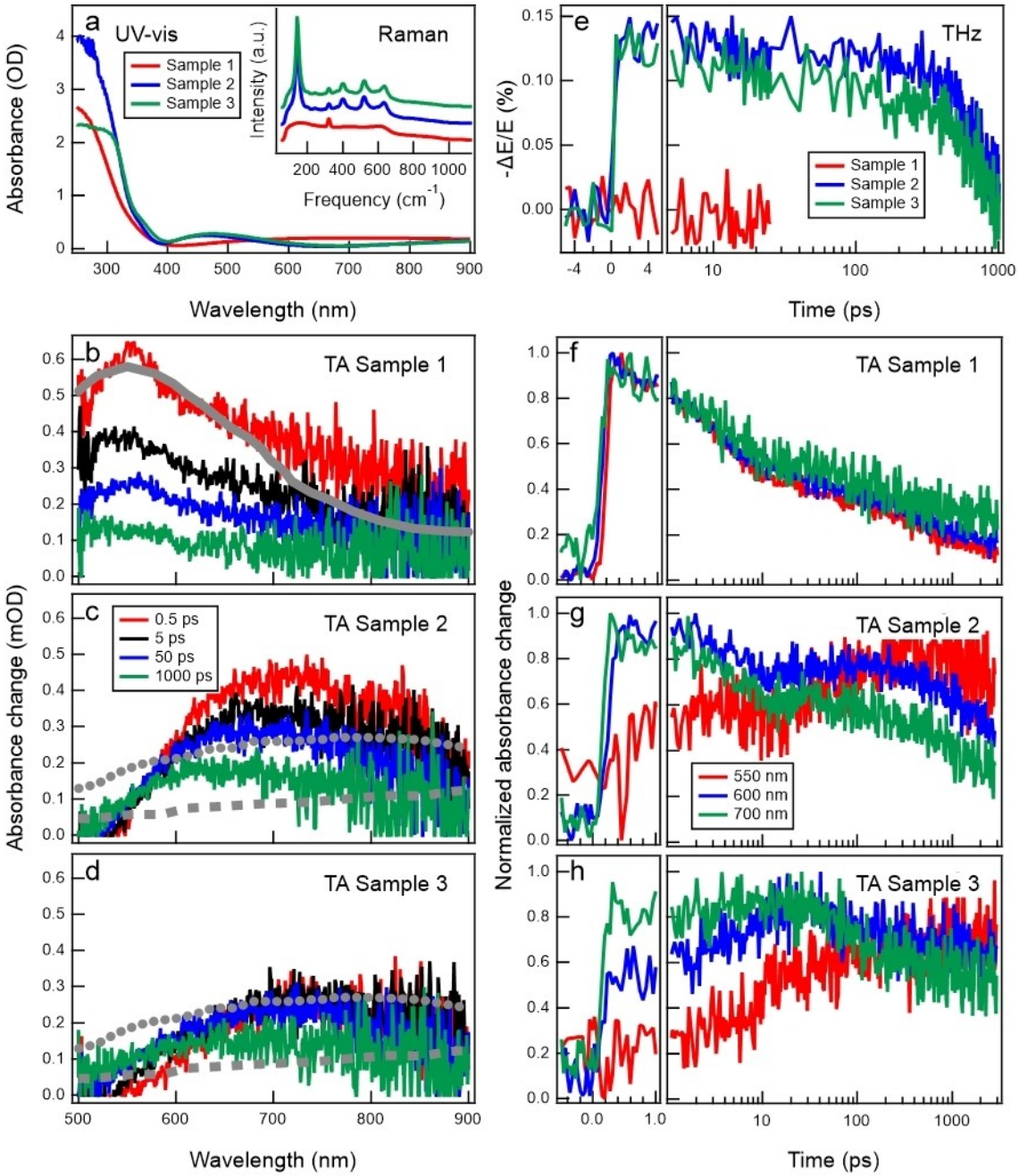

Figure 1. (a) UV/Vis absorption spectrum of three different TiO_2 films deposited on 2 mm thick CaF_2. The absorbance of CaF_2 in this wavelength range is negligible. The TiO_2 films are in contact with air. The inset shows Raman spectra for the three different TiO_2 films. The peak at 319 cm^{-1} originates from the CaF_2 substrate. The sharp resonances observed for samples 2 and 3 indicate the presence of crystalline regions, whereas sample 1 appears purely amorphous. The spectra are normalized to the region between 800 and 1000 cm^{-1} and offset for clarity. (b)-(d) Differential absorption spectra after excitation at 315 nm at selected time points for the three different TiO_2 samples in contact with air. An absorbance of 0.4 mOD corresponds to a transmission of 99.9%. The solid grey line in panel b represents the response for trapped holes reported in Ref. [21]. The grey lines in both panels c and d represent the response for trapped (dotted) and conducting (dashed) electrons reported in Ref. [21]. Reprinted from Chem. Phys. Lett., Vol 500, R. Katoh et al., "Transient absorption spectra of nanocrystalline TiO_2 films at high excitation density", Pages 309–312, Copyright (2010), with permission from Elsevier. (e) THz photoconductivity (proportional to the relative pump-induced change in the THz fields $-\frac{\Delta E}{E}$) after excitation at 310 nm for the three different TiO_2 samples in contact with air. (f)-(h) Normalized absorbance change as a function of time at 550, 600, and 700 nm for the three different samples.

details can be found in the SI. The transient spectra for the three different samples at selected time points are depicted in Figure 1b–d. The TA data show no signal before time zero, and no corrections are performed. Interestingly, the behavior of sample 1 is very different from samples 2 and 3. Sample 1 has a maximum in the spectrum around 550 nm

and a long tail towards longer wavelengths. With increasing excitation-probe delay, the intensity gets smaller, but the spectral shape does not substantially change. In contrast, samples 2 and 3 have a broad positive signal with a maximum around 700 nm. Upon increasing delay time, the spectrum shifts slightly to shorter wavelengths. Comparing the spectral shape to literature results (grey lines, Figure 1b–d),[21,22] we conclude that the TA spectrum of sample 1 reflects trapped holes, while the spectrum of samples 2 and 3 is more similar to the response reported for trapped electrons. Combining this difference in the TA with the observed difference in the Raman spectra, indicates that the amorphous film (sample 1) has trapped holes, while the more crystalline samples (sample 2 and 3) are dominated by trapped electrons. The presence of small amount of Si and Al in sample 3 seem not to significantly influence the behavior. We note that the TA spectra reported in the literature mainly report on nanocrystalline (anatase TiO_2) films, and we study both amorphous and party crystalline layers. The comparison seems justified by the strong resemblance between the optical properties of amorphous TiO_2 and that of crystalline anatase TiO_2.[24,25] The instantaneous rise of the signal (<0.3 ps; Figure 1f–h) observed for all three samples agrees with literature reporting that the laser-induced generated free electron and holes are trapped within around 100 to 200 fs at surface-trapped states in nanoparticles and nanocrystalline films.[26–29] As such, we conclude that surface-trapped holes dominate sample 1, while samples 2 and 3 have predominantly surface-trapped electrons. Quantifying the amount of surface-trapped holes or surface-trapped electrons is difficult, as the spectra in the literature agree on the major trends, but differ in the details. As such, we did not perform a deconvolution of our spectra.

Some free charge carriers might remain in the bulk, but they give a signature outside our window in the IR region.[27] These can be detected by terahertz spectroscopy, a contact-free tool that can provide short-range electrical properties (carrier mobility over tens of nm) of photogenerated charge carriers.[30,31] In line with the TA result, THz photoconductivity measurements also unveil a major difference between sample 1 and samples 2 and 3: as shown in Figure 1e, no significant THz conductivity is observed for the former, while a THz signal is clearly observed for the latter. This signal decays on a 500–1000 ps timescale. We assign this difference to the difference in structure: a crystalline sample is generally expected to have a higher mobility than an amorphous material due to the larger disorder in the latter and the associated enhanced scattering and trapping of charges.[32,33]

The dynamics in the TA signals (Figure 1f–h) are difficult to interpret, as several species, e.g., small signals from free electrons, might contribute to the observed changes. The homogeneous kinetics observed for sample 1 shows that the TA spectrum of sample 1 is dominated by a single species, i.e., the surface-trapped holes. The more complex dynamics for samples 2 and 3 hints at a more mixed response dominated by surface-trapped electrons and contributions from free electrons and holes. As suggested in the literature, the slow decay in the TA signal observed for all three samples (Figure 1f–h) is probably a sign of the relaxation of surface-trapped electrons into deep bulk trapping sites.[34] Literature has reported that the dynamics are fluence-dependent[21,35] and depend on the state of the material,[36,37] with slower dynamics reported for crystalline TiO_2, which is in line with our observations. However, directly comparing our dynamics with literature is very difficult.

To determine the role of the surface-trapped holes on photocatalytic reactions occurring at the interface, we select sample 1 to perform SFG experiments in the O–H stretch region, monitoring water and its fragments. Before we discuss the time-resolved SFG data, we look into the static spectra to determine which surface species are present (see Supporting Information for experimental details). Figure 2a shows the static SFG spectra in the O–H stretch vibrational region for the thin film of 75 nm atomic layer deposited TiO_2 (sample 1) in contact with D_2O and H_2O of different pD/pH, respectively. We use the pH as a variable to tune the surface charge of the TiO_2 film. The pH 3 and 11 solutions have respectively 1 mM HCl and NaOH present with a corresponding Debye length of 9.5 nm. pH 7 marks the sample with Millipore water used as received. To avoid absorption of the IR light by water, the IR and visible beam travel through the TiO_2 film towards the TiO_2-water interface (see Figure 2b). By measuring in the O–H stretch region with D_2O in the cell, one would expect to detect only a frequency-independent nonresonant contribution to the SFG signal from TiO_2 and/or water. However, the D_2O spectra show small frequency-dependent features, indicating the presence of a tiny amount of trapped water in the TiO_2 film or between the TiO_2 film and the CaF_2 substrate.[15] As expected, the H_2O spectra have a substantially higher intensity than the D_2O spectra and show clear resonant features between 3000 and 3500 cm^{-1} with spectral shapes depending on the pH of the solution. Fitting the data with the commonly used model based on a complex nonresonant contribution and a sum of complex Lorentzian lineshapes (see e.g.[15]), suggests that we can describe the data with a small nonresonant contribution and three resonant peaks. In ref. [15], the assignment of the different signals is discussed in detail based on isotopic dilution and varying salt concentration experiments. Briefly, the data can be described with three resonances, of which the parameters are summarized in Table 1. The low-frequency peak, located around 3050 cm^{-1}, originates from O–H species pointing with H towards the surface. The low vibrational frequency indicates that this O–H group forms a strong hydrogen bond within the interfacial region with, for example, the oxygen of Ti–OH or Ti–O^-; See the species marked with the orange circle in Figure 2c corresponding to the orange shaded frequency range in Figure 2a. The high-frequency band around 3530 cm^{-1} is assigned to Ti–OH groups (purple shades and marks in Figure 2a and 2c, respectively). The amplitude of the middle-frequency band, around 3200–3350 cm^{-1}, flips sign around pH 5.[15] Below pH 5, this band originates from O–H groups pointing with the H atom down to the bulk, assigned in Ref [15] to water molecules in the near-surface region aligned by a positive surface charge on

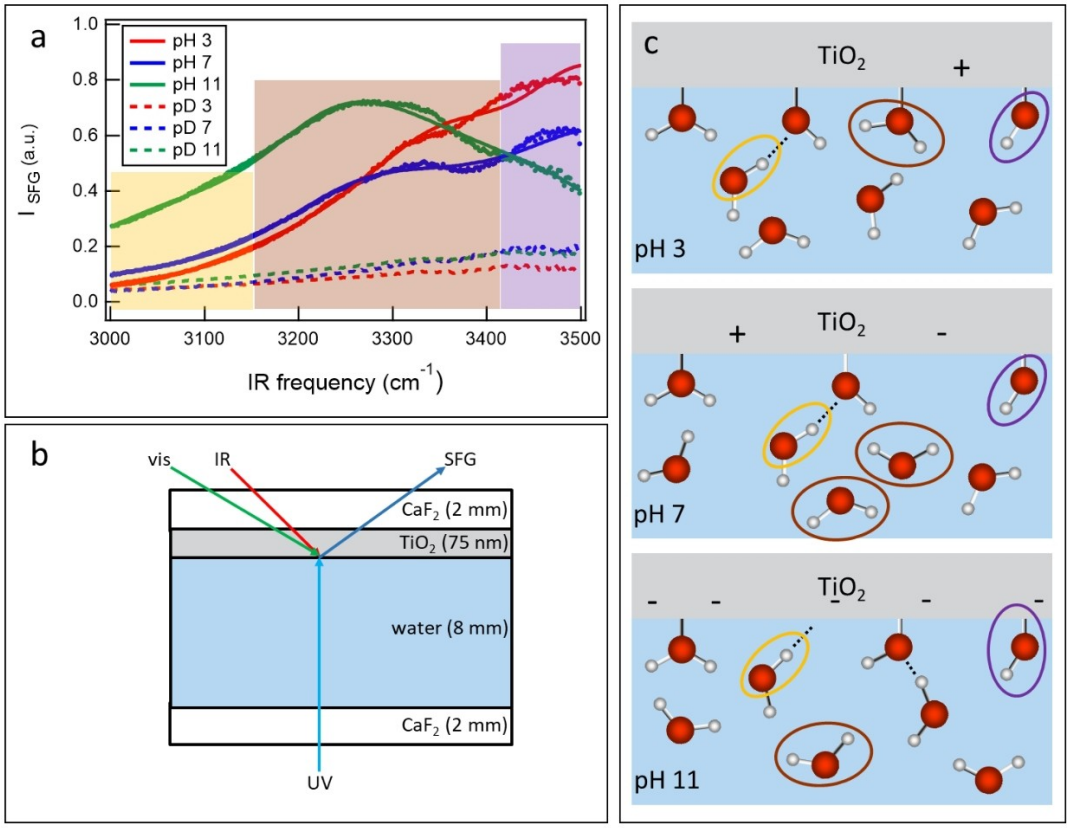

Figure 2. (a) SFG spectra in the O–H stretch vibrational region for D_2O (nonresonant response; dashed lines) and H_2O (combined resonant and nonresonant response; dots are experimental data, lines are fits with a Lorentzian lineshape model) in contact with amorphous TiO_2. The shaded areas correspond to the different interfacial OH groups marked with circles in panel c. (b) Schematic representation of the UV-pump, SFG-probe experiments. (c) Cartoon of the interfacial region in dependence of pH, for the acidic (top), the close to neutral (middle), and the basic (bottom) case. Circles indicate the vibrational frequencies in the SFG spectrum of panel a (orange: low-frequency; brown: central-frequency; purple: high-frequency), see also Table 1. For simplicity, the counter ions are omitted.

Table 1: Fit parameters with the commonly used SFG equation (see, for example, ref[15]) consisting of a nonresonant contribution and three Lorentzian lineshapes (characterized by its central frequency and full width at half maximum (FWHM)) together with the assignment of the resonant contributions, also marked with orange, brown, and purple in Figure 2.

		pH 3	pH 7	pH 11
I	O–H orientation	H towards TiO_2	H towards TiO_2	H towards TiO_2
	Frequency (cm^{-1})	3079	3050	3037
	FWHM (cm^{-1})	200	250	315
	Assignment	Water strongly hydrogen bonding over the H-atom with interfacial oxygen atoms		
II	O–H orientation	H away from TiO_2	H towards TiO_2	H towards TiO_2
	Frequency (cm^{-1})	3357	3246	3223
	FWHM (cm^{-1})	269	300	282
	Assignment	Ti–OH_2 and water below the possibly slightly positively charged TiO_2	Water below the negatively charged TiO_2	
III	O–H orientation	H away from TiO_2	H away from TiO_2	H away from TiO_2
	Frequency (cm^{-1})	3504	3542	3567
	FWHM (cm^{-1})	230	250	243
	Assignment	Ti–OH		

TiO_2. However, this signal could also be caused by Ti–OH_2 groups that may be partially positively charged.[38] A dominance of neutral Ti–OH_2 groups in the signal could explain the independence of the SFG data on the salt concentration, as discussed in Ref. [15]. Above pH 5, the main contribution to this band at 3200–3350 cm^{-1} comes from water molecules aligned with their H towards the TiO_2 due to the negative surface charge resulting from the pH-

induced deprotonation of the surface. As described in Ref. [15], more than 70 % of these water molecules are expected to be close to the interface and only up to 30 % in the diffuse layer. Of course, we cannot exclude that also a signal from Ti–OH_2 molecules is present with an opposite sign at roughly the same frequency. This type of water is marked with brown circles in Figure 2c, corresponding to the brown-shaded frequency range in Figure 2a.

As a first step in unraveling the mechanism of the photocatalytic water splitting, we irradiate the TiO_2 film (sample 1) with a short (sub-ps) 310 nm laser pulse and follow the changes in the SFG spectrum in the O–H stretch region. As the TiO_2 film has a strong absorbance at 310 nm (Figure 1a), it absorbs a significant amount of the incident light. Therefore, to excite the TiO_2 at the water side of the film, the UV light has to penetrate from the water side, resulting in the geometry depicted in Figure 2b. The absorbance of water[39] and CaF_2 at 310 nm is negligible.

Figure 3 shows the ratio of the excited and unexcited spectra $R(t)$ for specific times t for the three pH solutions. Before time zero, $R(t) = 1$, as the excitation pulse arrives at the sample after the probe. Around time zero, for pH 7 and pH 11, $R(t) < 1$, indicating that, upon exciting the TiO_2 with UV light, the SFG signal is reduced. The deviation from 1 gets smaller with increasing delay time. The signal for pH 11 at long delay time, i.e. 90 and 400 ps, turns above 1 at high frequency: the SFG signal is enhanced by the excitation. In contrast, the signal at pH 3 has a different behavior: the signal is close to 1 around time zero and gets increasingly smaller than 1. To obtain information about the timescale of the dynamics, Figure 4a shows the integrated signal between 3100 and 3400 cm^{-1} for the different solutions. We chose these integration limits because the data have a higher noise level below 3100 cm^{-1} and above 3400 cm^{-1}. For pH 7 and 11, the signal drops immediately after UV excitation, which is clear from the signal being significantly smaller than 1 at t = 0.1 ps. Subsequently, for pH 11, the ratio of the excited and unexcited signal increases, while for pH 7, the ratio remains more or less constant. The pH 3 data show an initial signal very close to 1 changing to roughly 0.9 at 100 ps.

As mentioned above, the SFG signal consists of nonresonant and resonant contributions. We can independently measure the time-dependent nonresonant signal by performing UV excitation SFG-probe experiments with D_2O at different pDs in the cell. We expect—if any—only a minor contribution from the trapped water, as the UV excitation is at most only weakly affecting these water molecules, as they are located far from the TiO_2-D_2O interface—the interface we excite with the UV light. The measured absorbance of around 1.2 OD at 310 nm (see Figure 1a) indicates that only 6 % of the light is transmitted through the TiO_2 film and thus reaches the CaF_2–TiO_2 interface. As shown in Figure 4b, the nonresonant signal changes instantaneously for all pH values and decays with a timescale of a few hundred picoseconds. The signal intensities, but not the dynamics, are pD-dependent. Moreover, the dynamics are clearly different from the fast dynamics observed for the resonant signals in Figure 4a.

A likely origin of the time-dependent response of the nonresonant signal measured with the D_2O samples is the DC field induced by the trapped holes at the surface. Such fields could polarize TiO_2 and D_2O differently, changing the static nonresonant signal and thus inducing a change in the SFG signal. In this scenario, the trapped holes in the near-surface region recombine with electrons on a 500 ps timescale.

To obtain a mechanistic picture of the interfacial molecular processes detected with SFG, we describe our data with a phenomenological model. As mentioned above in describing the SFG spectra depicted in Figure 2, the different pH data are fitted with the commonly used Lorentzian lineshape model using three resonant modes with the sign of the amplitudes being opposite for O–H groups with the H atom towards or away from the TiO_2 as

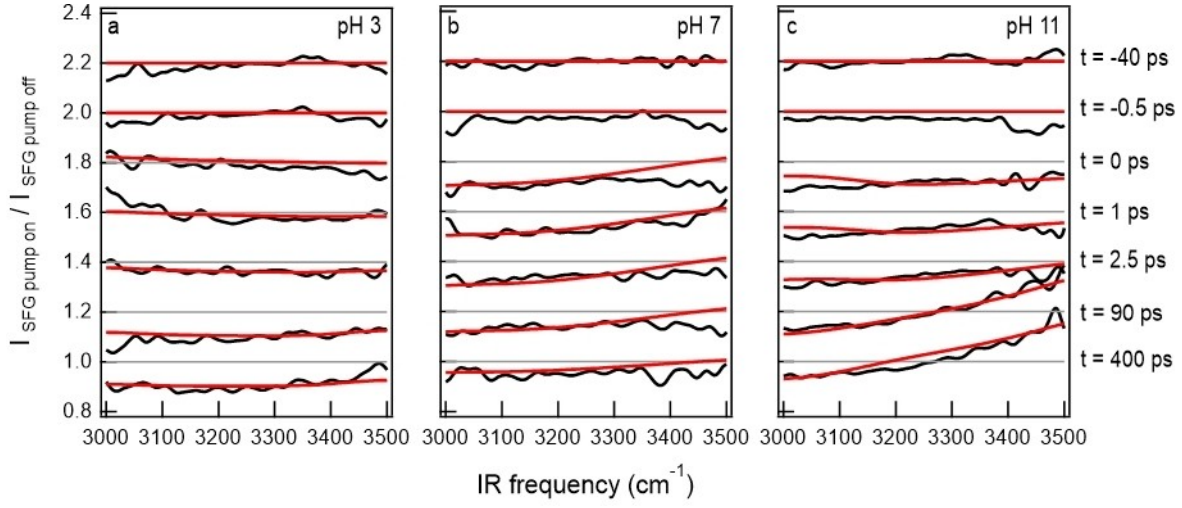

Figure 3. SFG ratio spectra in black at several delay times showing the spectral changes upon exciting the TiO_2 with UV light of 310 nm for TiO_2 in contact with water of pH 3 (a), pH 7 (b), and pH 11 (c). The data have an offset of 0.2 between each spectrum for clarity, with grey zero lines. The red curves are the SFG ratio spectra obtained from the model described in the text.

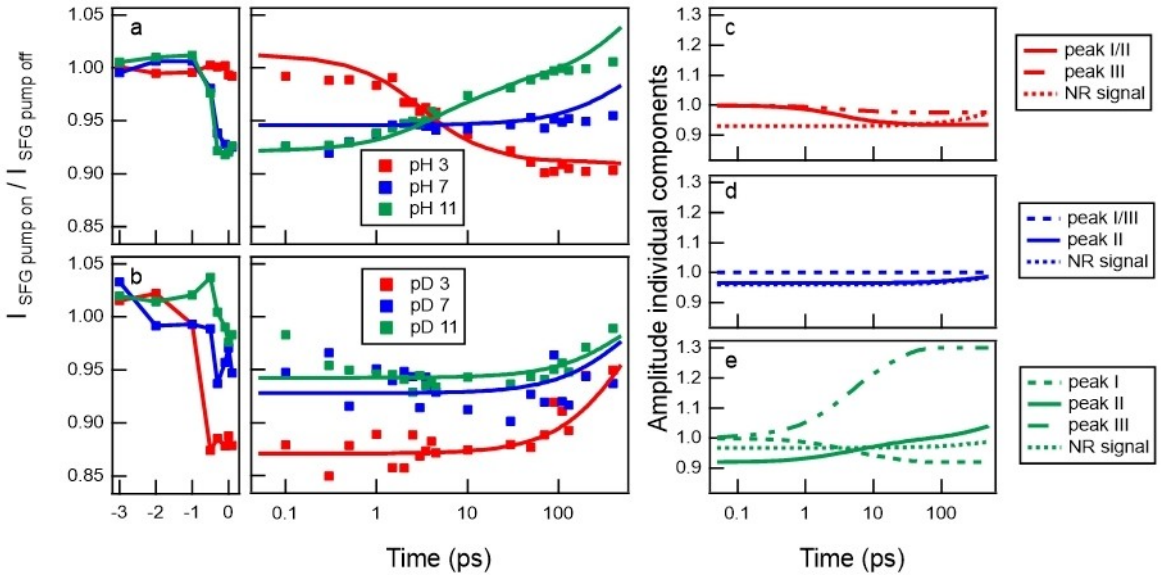

Figure 4. Integrated ratio of the excited and unexcited SFG spectra between 3100 and 3400 cm^{-1} as a function of time (left: linear for very early times; right: logarithmic) between excitation and probe pulses for (a) the H_2O–TiO_2 (combined resonant and nonresonant response) interface at varying pH and (b) the D_2O–TiO_2 (nonresonant response) interface at varying pD. The lines in the right column are the integrated ratios obtained from the model described in the text. Please note that as depicted in Figure 2, the SFG signals for the D_2O case are an order of magnitude smaller than the SFG signals for the H_2O case resulting in the more prominent noise in panel b. (c)–(e) Time-dependence of the amplitude of the resonant and nonresonant contribution for pH 3, pH 7, and pH 11.

summarized in Table 1. Besides, a small nonresonant signal is included in the model. Subsequently, we assume certain dynamics (i.e., timescale and amplitude change) for the nonresonant and the resonant signal as described below for the different cases. Time-resolved SFG spectra are then calculated, divided by the modeled SFG spectrum under steady-state conditions like in the experiment, and subsequently integrated between 3100 and 3400 cm^{-1}. To describe the time-resolved data, we first model the nonresonant response from the D_2O data (see Figure 4b): the nonresonant signal changes instantaneously upon excitation, and relaxes on a 500 ps timescale. The solid lines in Figure 4b are obtained with this simple model in which only the amplitude of the change in nonresonant signal was adapted to match the data. For the H_2O samples, the change in the amplitude of the nonresonant signal was taken from the corresponding D_2O result for each pH. Besides, now also the resonant signals assigned to different types of O–H groups might change in amplitude. In describing the results, we first focus on the initial signal at $t = 0$ ps. With this scenario of using the magnitude and sign of the change in the nonresonant signal, also for the resonant case, the pH 3 data at time zero could be perfectly described without the need to include a change in the resonant response. The quasi-instantaneous decrease of the SFG signal observed for D_2O is absent in the spectrum for H_2O at pH 3, which can be traced to the interference between the excitation-pulse perturbed nonresonant and unperturbed resonant signals. For pH 7 and 11, an additional instantaneous decrease in the signal for peak II, the signal originating from water molecules below the negatively charged TiO_2 is necessary to describe the H_2O results at time zero. This instantaneous signal reflects a change of surface potential due to a change in surface charge due to the rapid generation of electrons and holes. The potential change affects the water molecules' electronic polarization, changing their SFG signal without a physical rearrangement of the molecules. The decrease in the signal indicates a reduction of the surface charge. As the surface is negatively charged at pH 7 and 11 under static conditions, we conclude thus that upon irradiation, positive charges, i.e. holes, are dominantly present at the surface. This is in agreement with the conclusion drawn above from the TA experiments. As peak II in the pH 3 case most likely predominantly originates from water molecules binding to TiO_2, this signal is not sensitive to the change of surface charge. Besides this instantaneous signal, we assume in the model that independent of the pH, each of the three resonant signals, as assigned in Table 1, exhibit biexponential dynamics on a 3 and 16 ps timescale. The changes in amplitudes of the three resonances are adapted such that the model describes the data, as is depicted in Figure 3 (red lines) for the full spectral range between 3000 and 3500 cm^{-1} and Figure 4 (solid lines in the right panel) for the integrals between 3100 and 3400 cm^{-1}. The resulting change in the amplitudes of the different signals is summarized in Table 2 and graphically in Figure 4c–e. For pH 3, the amplitude of all peaks decreases, while for pH 11, the amplitude of the low-frequency peak decreases, and the amplitude of the other two peaks increases. Besides the instantaneous change in peak II, no additional change in the resonant signal for pH 7 has to be considered.

This simple model describes the data very well, as evidenced by the good quality of the fits seen in Figure 3 and 4. It captures both the spectral and temporal shape and

Table 2: Results of the model to describe the UV excitation SFG-probe data. I, II, and III refer to the assignment in Table 1, also marked with orange, brown, and purple in Figure 2.

		pH 3	pH 7	pH 11
NR	Amplitude change	−7%	−4%	−3.25%
I	Amplitude change on 3 and 16 ps timescale	−6.5%	–	−8%
II	Instantaneous change	–	−3.5%	−8%
	Amplitude change on 3 and 16 ps timescale	−6.5%	–	+7%
III	Amplitude change on 3 and 16 ps timescale	−2.5%	–	+30%
	Ratio 3 ps to 16 ps component	0.7 to 0.3	–	0.5 to 0.5

the difference between the nonresonant pD and the combined resonant and nonresonant pH data. By combining Tables 1 and 2, we obtain the following picture of the dynamics at the interface, schematically depicted in Figure 5. At pH 3, all peaks reduce in intensity. As the intensity of the low-frequency peak is very low to begin with, we will not conclude anything about the change in this peak. The decrease in the middle and high-frequency peaks shows a reduction of the interfacial Ti–OH_2 (and/or oriented water with H away from the surface in the near-surface region) and the Ti–OH species, due to a deprotonation reaction (Figure 5 top, solid, and dashed green circle, respectively), as proposed in the literature (e.g.[9,10]). In principle, deprotonation of the Ti–OH_2 band (peak II) should increase the Ti–OH band (peak III), but apparently, the further deprotonation of the Ti–OH band dominates (Figure 5 top, dashed circle). A deprotonation of the Ti–OH band could, in some cases (no consumption of holes), result in Ti–O^- and thus a decrease of a potentially positive surface charge, which would also explain the slight reduction in the middle-frequency peak amplitude. At pH 11, the most prominent change is the 30% increase in the Ti–OH peak amplitude combined with a moderate increase of 7% of the middle-frequency peak and a decrease in the low-frequency peak amplitude. The Ti–OH peak increase can be assigned to hole-induced water dissociation in the near-surface area (Figure 5 bottom, green solid circles). At this relatively high pH, the resulting protons will most likely react with OH^- to form water molecules. Following the instantaneous decrease immediately after the excitation, the increase in the middle-frequency peak hints at a subsequent increase in the surface charge on a 3 and 16 ps timescale aligning the water molecules in the interfacial region. This increase in surface charge is tentatively assigned to a reaction between Ti–OH groups and OH^- present in the aqueous phase at high pH, resulting in Ti–O^- and H_2O (Figure 5 bottom, green dotted circles).

The reaction mechanism is remarkably similar at pH 3 and 11: our spectroscopy indicates that H_2O is converted to Ti–OH groups, and pre-existing Ti–OH groups to Ti–O groups, possibly negatively charged. This conversion from water into Ti–OH, observed here for the first time experimentally at the TiO_2-water interface in the presence of bulk amounts of water, has been predicted by theoretical studies as the first step in photocatalytic hydrogen generation.[9,10,12,40] Although our experimental data are for amorphous TiO_2, we might compare them to literature results for anatase, as the optical properties of amorphous TiO_2 and anatase strongly resemble each other.[24,25] Another justification might be the good match between the TA spectra with literature as shown in Figure 1. As mentioned in the introduction, Chen et al. proposed that in the overall proton-coupled electron transfer reaction at low pH, i.e., $Ti–OH_2 + h^+ \rightarrow Ti–OH + H^+$, the proton transfer step

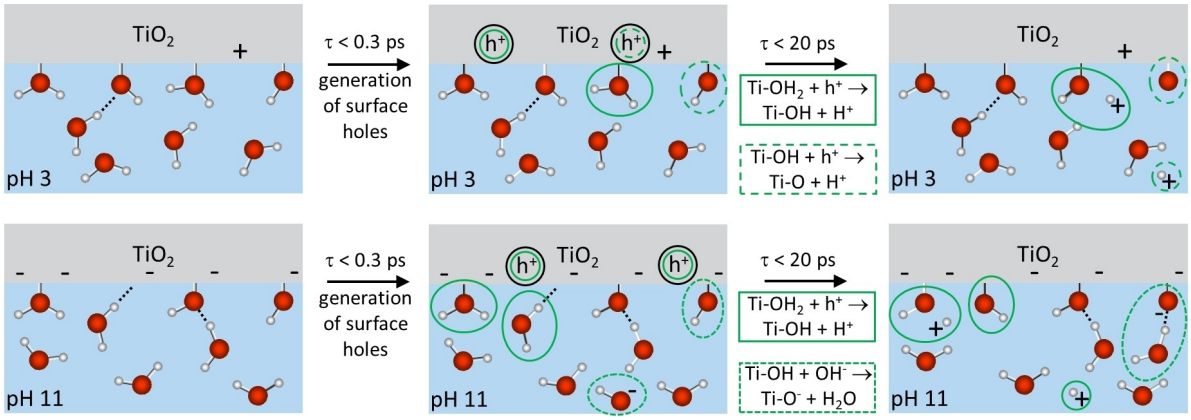

Figure 5. Schematics of the photo-induced processes at the interface between the photocatalyst TiO_2 and an aqueous solution of pH 3 (top) and pH 11 (bottom). The left-to-middle panels show the generation of the holes, while the middle-to-right panels sketch the different reactions that are observed at the interface. The green solid and dashed lines in the middle and right panels represent the two reactions shown between the panels. At both pH 3 and 11, the holes initiate deprotonation of water in the near-surface region (green solid circles). At pH 3, the holes also mediate the deprotonation of Ti–OH groups (green dotted circles). At pH 11, Ti–OH groups might react with OH^- to Ti–O^- (green dotted circles). See the main text for more details.

$Ti–OH_2 \rightarrow Ti–OH^- + H^+$ is rate-limiting, while at high pH, it is the electron transfer reaction $Ti–OH^- + h^+ \rightarrow Ti–OH$.[10] Their study predicted a significantly lower barrier for electron than for proton transfer, so they concluded that, at high pH, the reaction should be faster. In our experiments, we find similar timescales for the reaction at pH 3 and 11, which is in agreement with a recent theoretical study by Ma et al. concluding that an internal hydrogen bonding network can assist the coupled hole and proton transfer, substantially reducing the barrier compared to the situation of isolated water molecules.[12] Interestingly, the sub-20 ps timescale observed in our work is on the same order of magnitude as the timescale observed for hole-mediated dissociation in a theoretical study by Han et al.. They observe an increase in the water coverage on the anatase surface about 4 ps after hole trapping and water dissociation roughly 8 ps after hole trapping.[41]

Conclusion

In summary, we have presented experimental evidence for photocatalytic water dissociation at the interface between water and TiO_2 in the realistic scenario of room temperature and the presence of bulk water. After excitation with UV light, for the first time, we experimentally show that following the quasi-instantaneous surface hole generation by light absorption, the initial water dissociation steps involve hole-assisted deprotonation of near-surface water molecules (into Ti–OH intermediates) and/or hydroxyl groups attaching to the surface. The interfacial processes occur on a timescale best described with a biexponential with time constants of 3 and 16 ps. Knowledge of these timescales is important, since the desired reaction pathway competes with other processes, such as recombination and trapping of photogenerated charge carriers, as well as competing, unwanted chemical reactions. Knowledge of these rates allows for optimizing the system for the desired pathway, by accelerating that pathway and/or slowing down undesired processes. As such, the ability to measure reaction rates directly, as presented here, is quintessential for designing improved catalysts based on fundamental insights rather than through trial and error.

Author Contributions

E.H.G.B. and M.B. conceived the research idea. M.G. and A.D. prepared the samples. S.H., S.S., and S.J.S. performed the SFG experiments, C.R. the TA experiments, M.Z. and E.H.G.B. the UV-vis and Raman experiments, and X.J. and H.I.W. the THz measurements. E.H.G.B. analyzed the SFG data and modeled the SFG dynamics. C.R. and E.H.G.B. analyzed the TA experiments, while Y.J., H.I.W., and E.H.G.B. analyzed the THz data. E.H.G.B. and M.B. wrote the manuscript. All authors discussed the results.

Acknowledgements

The authors thank Stefan Weber, Ulmas Zhumaev, Maksim Grechko, Shuai Fu, Johannes Hunger, and Julia Völkle for valuable comments and discussions, Malte Deiseroth for help with data analysis, and Moritz Eder, Gareth Parkinson and Markus Sauer from TU Wien for the XPS experiments and discussion. The authors also acknowledge the use of facilities at the Analytical Instrumentation Center (AIC), TU Wien, Austria. This research was supported by the Austrian Science Fund (FWF, SFB Project ′TACO′, F81) and an ERC Starting Grant (Grant No. 336679).

Conflict of Interest

The authors declare no conflict of interest.

Data Availability Statement

The data that support the findings of this study are available from the corresponding author upon reasonable request.

Keywords: Interface · Photocatalyst · Sum Frequency Generation · Time-Resolved Spectroscopy · Titanium Dioxide

[1] A. Fujishima, K. Honda, *Nature* **1972**, *238*, 37–38.
[2] Q. Wang, K. Domen, *Chem. Rev.* **2020**, *120*, 919–985.
[3] S. Chen, T. Takata, K. Domen, *Nat. Rev. Mater.* **2017**, *2*, 17050.
[4] H. Eidsvåg, S. Bentouba, P. Vajeeston, S. Yohi, D. Velauthapillai, *Molecules* **2021**, *26*, 1687.
[5] U. Diebold, *Surf. Sci. Rep.* **2003**, *48*, 53–229.
[6] M. A. Henderson, *Surf. Sci. Rep.* **2011**, *66*, 185–297.
[7] Q. Guo, Z. Ma, C. Zhou, Z. Ren, X. Yang, *Chem. Rev.* **2019**, *119*, 11020–11041.
[8] M. Z. Rahman, T. Edvinsson, J. Gascon, *Nat. Chem. Rev.* **2022**, *6*, 243–258.
[9] Á. Valdés, Z.-W. Qu, G.-J. Kroes, J. Rossmeisl, J. K. Nørskov, *J. Phys. Chem. C* **2008**, *112*, 9872–9879.
[10] J. Chen, Y. F. Li, P. Sit, A. Selloni, *J. Am. Chem. Soc.* **2013**, *135*, 18774–18777.
[11] D. Wang, T. Sheng, J. Chen, H. F. Wang, P. Hu, *Nat. Catal.* **2018**, *1*, 291–299.
[12] X. Ma, Y. Shi, J. Liu, X. Li, X. Cui, S. Tan, J. Zhao, B. Wang, *J. Am. Chem. Soc.* **2022**, *144*, 13565–13573.
[13] S. Kataoka, M. C. Gurau, F. Albertorio, M. A. Holden, S. M. Lim, R. D. Yang, P. S. Cremer, *Langmuir* **2004**, *20*, 1662–1666.
[14] S. Hosseinpour, F. Tang, F. Wang, R. A. Livingstone, S. J. Schlegel, T. Ohto, M. Bonn, Y. Nagata, E. H. G. Backus, *J. Phys. Chem. Lett.* **2017**, *8*, 2195–2199.
[15] S. J. Schlegel, S. Hosseinpour, M. Gebhard, A. Devi, M. Bonn, E. H. G. Backus, *Phys. Chem. Chem. Phys.* **2019**, *21*, 8956–8964.
[16] I. M. Nadeem, J. P. W. Treacy, S. Selcuk, X. Torrelles, H. Hussain, A. Wilson, D. C. Grinter, G. Cabailh, O. Bikondoa, C. Nicklin, A. Selloni, J. Zegenhagen, R. Lindsay, G. Thornton, *J. Phys. Chem. Lett.* **2018**, *9*, 3131–3136.
[17] A. Barybin, V. Shapovalov, *Int. J. Opt.* **2010**, *2010*, 137572.
[18] P. Romero-Gómez, V. Rico, A. Borrás, A. Barranco, J. P. Espinós, J. Cotrino, A. R. González-Elipe, *J. Phys. Chem. C* **2009**, *113*, 13341–13351.

[19] T. Ohsaka, F. Izumi, Y. Fujiki, *J. Raman Spectrosc.* **1978**, *7*, 321–324.
[20] T. Faraz, H. C. M. Knoops, M. A. Verheijen, C. A. A. van Helvoirt, S. Karwal, A. Sharma, V. Beladiya, A. Szeghalmi, D. M. Hausmann, J. Henri, M. Creatore, W. M. M. Kessels, *ACS Appl. Mater. Interfaces* **2018**, *10*, 13158–13180.
[21] R. Katoh, M. Murai, A. Furube, *Chem. Phys. Lett.* **2010**, *500*, 309–312.
[22] T. Yoshihara, R. Katoh, A. Furube, Y. Tamaki, M. Murai, K. Hara, S. Murata, H. Arakawa, M. Tachiya, *J. Phys. Chem. B* **2004**, *108*, 3817–3823.
[23] T. J. Miao, J. Tang, *J. Chem. Phys.* **2020**, *152*, 194201.
[24] B. Prasai, B. Cai, M. K. Underwood, J. P. Lewis, D. A. Drabold, *J. Mater. Sci.* **2012**, *47*, 7515–7521.
[25] A. Jolivet, C. Labbé, C. Frilay, O. Debieu, P. Marie, B. Horcholle, F. Lemarié, X. Portier, C. Grygiel, S. Duprey, W. Jadwisienczak, D. Ingram, M. Upadhyay, A. David, A. Fouchet, U. Lüders, J. Cardin, *Appl. Surf. Sci.* **2023**, *608*, 155214.
[26] S. Kohtani, A. Kawashima, H. Miyabe, *Catalysts* **2017**, *7*, 303.
[27] Y. Tamaki, K. Hara, R. Katoh, M. Tachiya, A. Furube, *J. Phys. Chem. C* **2009**, *113*, 11741–11746.
[28] J. Schneider, M. Matsuoka, M. Takeuchi, J. Zhang, Y. Horiuchi, M. Anpo, D. W. Bahnemann, *Chem. Rev.* **2014**, *114*, 9919–9986.
[29] X. Yang, N. Tamai, *Phys. Chem. Chem. Phys.* **2001**, *3*, 3393–3398.
[30] R. Ulbricht, E. Hendry, J. Shan, T. F. Heinz, M. Bonn, *Rev. Mod. Phys.* **2011**, *83*, 543–586.
[31] W. Zheng, B. Sun, D. Li, S. M. Gali, H. Zhang, S. Fu, L. Di Virgilio, Z. Li, S. Yang, S. Zhou, D. Beljonne, M. Yu, X. Feng, H. I. Wang, M. Bonn, *Nat. Phys.* **2022**, *18*, 544–550.
[32] G. W. Ludwig, R. L. Watters, *Phys. Rev.* **1956**, *101*, 1699–1701.
[33] A. R. Moore, *Appl. Phys. Lett.* **1977**, *31*, 762–764.
[34] Y. Tamaki, A. Furube, M. Murai, K. Hara, R. Katoh, M. Tachiya, *Phys. Chem. Chem. Phys.* **2007**, *9*, 1453–1460.
[35] J. Tang, J. R. Durrant, D. R. Klug, *J. Am. Chem. Soc.* **2008**, *130*, 13885–13891.
[36] R. Khan, H. Ali-Löytty, J. Saari, M. Valden, A. Tukiainen, K. Lahtonen, N. V. Tkachenko, *Nanomaterials* **2020**, *10*, 1567.
[37] J. Saari, H. Ali-Löytty, M. M. Kauppinen, M. Hannula, R. Khan, K. Lahtonen, L. Palmolahti, A. Tukiainen, H. Grönbeck, N. V. Tkachenko, M. Valden, *J. Phys. Chem. C* **2022**, *126*, 4542–4554.
[38] P. A. Connor, K. D. Dobson, A. James McQuillan, *Langmuir* **1999**, *15*, 2402–2408.
[39] J. D. Mason, M. T. Cone, E. S. Fry, *Appl. Opt.* **2016**, *55*, 7163.
[40] Y. F. Li, Z. P. Liu, L. Liu, W. Gao, *J. Am. Chem. Soc.* **2010**, *132*, 13008–13015.
[41] F. Han, L. Zhu, Z. Huang, Z. Zhou, *J. Phys. Chem. Lett.* **2020**, *11*, 7590–7594.

Manuscript received: August 18, 2023
Accepted manuscript online: November 27, 2023
Version of record online: January 12, 2024